Multiconfiguration self-consistent-field *ab initio* and local-density-functional studies on the vibrational structure of core-level photoelectron spectra of SiH_4 and GeH_4

Z. F. Liu* and G. M. Bancroft†
Department of Chemistry, The University of Western Ontario, London, Ontario, Canada N6A 5B7
Canadian Synchrotron Radiation Facility, Synchrotron Radiation Center, University of Wisconsin, Stoughton, Wisconsin 53589

J. S. Tse†
Steacie Institute for Molecular Sciences, National Research Council of Canada, Ottawa, Ontario, Canada K1A 0R6

Hans Ågren
Institute of Physics and Measurement Technology, University of Linköping, S-58183, Linköping, Sweden
(Received 2 August 1994)

The periodic trends in the vibrational structure of core-level photoelectron spectra are studied by multiconfiguration self-consistent-field *ab initio* and local-density-functional calculations on SiH_4 and GeH_4. Contributions from both symmetric stretching and bending vibrations to the vibrational structure are studied. These periodic trends are rationalized by the screening of the core charge, and in terms of electrostatic and relaxation contributions to core ionization, which determine the change in the M—H (M=Si,Ge) bond length.

PACS number(s): 33.60.Cv, 33.20.Wr, 31.15.Ew, 31.15.Ar

I. INTRODUCTION

The line shape in core-level photoelectron spectra is usually influenced by several factors, such as vibronic coupling, lifetime broadening, and ligand field splitting [1]. Careful consideration of these factors is necessary for a correct interpretation of core-level photoelectron spectra, especially for high-resolution studies which are now achievable with monochromatized synchrotron radiation.

Recently, gas-phase high-resolution studies [2–5] by our group have revealed periodic trends for the symmetric stretching mode vibrational structure in core-level photoelectron spectra [6]. Specifically, we found that the vibrational structure decreases dramatically down a group of congeneric molecules (e.g., from CH_4 to SiH_4 to GeH_4) and across a periodic row of isoelectronic molecules (e.g., from SiH_4 to PH_3 to H_2S) [6]. Such qualitative trends can help us to assess the importance of vibrational splitting in a core-level spectrum and to interpret correctly the unresolved broadening often observed in the core-level spectra of solids and surfaces.

As a continuing part of our efforts to understand the vibrational structure in core-level photoelectron spectra, in this paper we report multiconfiguration self-consistent-field (MCSCF) *ab initio* [7,8] and local-density-functional [9] (LDF) calculations on the vibrational structure of the core levels of SiH_4 and GeH_4. We carried out these calculations with several goals in mind: to corroborate the assignments and observations in our previous studies; to study the deep core levels for which high-resolution experimental results are not yet available; to assess the contribution of bending mode vibrations; and, based on these results, to derive a qualitative explanation for the above-mentioned trends. In addition, by comparison with previous experimental results and with MCSCF *ab initio* results, we seek to assess the accuracy of the LDF method for the study of such vibrational structures. The significance of such an assessment lies in the possibility of using the LDF method to study the vibrational structure in the core-level excitations of large molecules, for which an *ab initio* calculation is too demanding.

II. COMPUTATIONAL DETAILS

MCSCF calculations were performed within the complete active space self-consistent field (CASSCF) approximation [7], using the SIRIUS program [8]. Results are displayed for basis sets of similar quality to that used in Asplund *et al.*'s calculation [10] for CH_4: $[12s8p/6s4p]$ plus d functions with an exponent of 0.6 for Si [11], $[13s9p5d/7s5p3d]$ for Ge [12], and $[4s/3s]$ for H [13]. Both SiH_4 and GeH_4 were calculated in C_{2v} symmetry, because the SIRIUS program can only handle the subgroups of D_{2h}. The complete active space [7] for the MCSCF expansion includes the core hole orbital, all occupied valence orbitals, and unoccupied orbitals with a natural orbital occupation number larger than 0.005. Specifically, for SiH_4 six unoccupied orbitals were included: four a_1 orbitals, one b_1 orbital, and one b_2 orbital. For GeH_4, nine unoccupied orbitals are included: four a_1 orbitals, two b_1 orbitals, two b_2 orbitals, and one a_2 or-

*Present address: Department of Chemistry, University of California, Berkeley, CA 94720.
†To whom correspondence should be addressed.

bital. The calculations of the core hole states using the MCSCF method followed the steps outlined in Ref. [8].

The potential-energy surface was obtained by varying the Si—H or Ge—H bond lengths. A MCSCF calculation was performed to obtain the corresponding total energy for each geometry. At least 15 points were calculated for each potential-energy surface. A step of 0.01 a.u. was used in the equilibrium region, and the error of equilibrium bond length calculated by the MCSCF method was within ±0.01 a.u. The relation between the total energy and the bond length was then fitted to a polynomial up to an exponent of 6. The energy polynomial was forced to be at a minimum at the equilibrium bond length. Vibrational wave functions and frequencies for symmetrical stretching were calculated by treating the cubic term and the terms above it as a perturbation [14]. The Franck-Condon factors [15] were then obtained by calculating the overlap integrals between the ground state and core hole state vibrational wave functions, expanded in Hermite polynomials. All integrals involving Hermite polynomials were calculated numerically.

The LDF calculations on SiH_4 and GeH_4 were carried out using the DMOL program obtained from Biosym [16]. Double numerical quality basis sets, with polarization functions added, were used for all three atoms. All the core orbital were unfrozen during the SCF iteration. The ground states were calculated using spin-restricted wave functions, while the core hole states were calculated using spin-unrestricted wave functions. The equilibrium bond lengths for the ground and the core hole states were calculated by geometrical optimization using the energy gradient [17]. The potential-energy surfaces and the Franck-Condon factors were calculated in the same way as in the MCSCF calculations.

III. RESULTS

A. SiH_4 Si 2p and GeH_4 Ge 3d calculations

The calculated (both MCSCF and LDF) ionization potentials and equilibrium bond lengths are listed in Table I, and the calculated Franck-Condon factors are listed in Table II. The vibronic coupling resolved in the experiment reported in Ref. [6] is due to the symmetric stretching vibrations. In other words, the vibrational structure is due to the change in the M—H bond length after the core-level ionization. The potential-energy surfaces for the ground state and the 2p core hole state of SiH_4, calculated by the MCSCF method, are shown on the left-hand side of Fig. 1. The bond length obtained for the ground state is 2.82 a.u., compared to the experimental value of 2.799 a.u. [18]. The bond length obtained for the 2p hole state is 2.72 a.u. Thus the Si—H bond contracts 0.1 a.u. after the 2p hole is created (Table I). The resultant Franck-Condon line shape, after taking account of the spin-orbit splitting of the 2p hole state, is shown in Fig. 2 (also see Table II). The agreement between theory and experiment is satisfactory. Using the same potential-energy surfaces, but changing the mass of the H atom to the D atom, the calculated Franck-Condon factor for SiD_4 is also in reasonable agreement with experiment [4] (Table II), and has reproduced the expected isotope effects.

In contrast, the bond-length difference between the GeH_4 ground state and the Ge 3d hole state is much smaller, with the Ge—H bond only 0.04–0.06 a.u. shorter after the Ge 3d ionization (Table I), according to the MCSCF results. Therefore the vibronic coupling effect is smaller for GeH_4 than for SiH_4 (Table II). Thus the

TABLE I. The ionization potentials and equilibrium bond lengths of SiH_4 and GeH_4 calculated by MCSCF and LDF methods.

Core-hole state	Symmetry	MCSCF IP (eV)	MCSCF M—H bond length (a.u.)	LDF IP (eV)	LDF M—H bond length (a.u.)
		SiH_4			
Ground	a_1		2.82		2.827
Si 1s	a_1	1851.3	2.67	1844.5	2.646
Si 2s	a_1	159.30	2.72	149.63	2.741
Si 2p[a]	t_2	107.03	2.72	108.62	2.734
		GeH_4			
Ground	a_1		2.90		2.904
Ge 1s	a_1	10 993	2.81	10 955	2.820
Ge 2s	a_1	1390.2	2.82	1364.0	2.853
Ge 2p	t_2	1233.4	2.82	1227.6	2.849
Ge 3s	a_1	186.41	2.84	170.29	2.878
Ge 3p	t_2	131.81	2.84	123.00	2.878
Ge 3d[b]	t_2	36.71	2.86	38.33	2.882
Ge 3d[b]	e	36.53	2.84	38.28	2.882

[a]Experimental ionization potential (IP) for Si 2p of SiH_4 is 107.32 eV.
[b]The experimental IP for Ge 3d of GeH_4 is 37.09 eV; both values are from Ref. [6].

TABLE II. Franck-Condon factors calculated by MCSCF and DMOL methods for SiH_4 and GeH_4.

Core-hole state	Vibrational splitting (eV) MCSCF	Vibrational splitting (eV) LDF	Franck-Condon factor (%) MCSCF $\nu'=0$	MCSCF $\nu'=1$	MCSCF $\nu'=2$	LDF $\nu'=0$	LDF $\nu'=1$	LDF $\nu'=2$
SiH_4 Si 2p[a]	0.304	0.316	72.3	24.5	2.6	72.9	23.4	3.1
SiH_4 Si 2s	0.329	0.315	70.5	24.9	4.0	76.4	20.9	2.3
SiH_4 Si 1s	0.333	0.334	44.7	37.3	13.6	29.3	37.9	21.2
SiD_4 Si 2p[b]	0.229	0.237	64.3	29.9	5.0	65.8	28.0	5.2
GeH_4 Ge 3d[c] (3d in t_2)	0.293	0.284	93.5	6.2	0.2	98.3	1.7	0.0
GeH_4 Ge 3d[c] (3d in e)	0.294	0.282	87.2	12.0	0.6	98.2	1.7	0.0
GeH_4 Ge 3p	0.295	0.282	87.3	11.9	0.6	97.6	2.4	0.0

[a]Experimental Franck-Condon factors for SiH_4 Si 2p are 66.3%, 29.1%, and 5.1%, and the vibrational freuquency is 0.295 eV [6].
[b]Experimental Franck-Condon factors for SiD_4 Si 2p are 53.6%, 34.5%, 9.6%, and 2.3%, and the vibrational frequency is 0.212 eV [5].
[c]Experimental Franck-Condon factors for GeH_4 Ge 3d are 91.5%, 8.5%, and 0.0%, and the vibrational frequency is 0.261 eV [6].

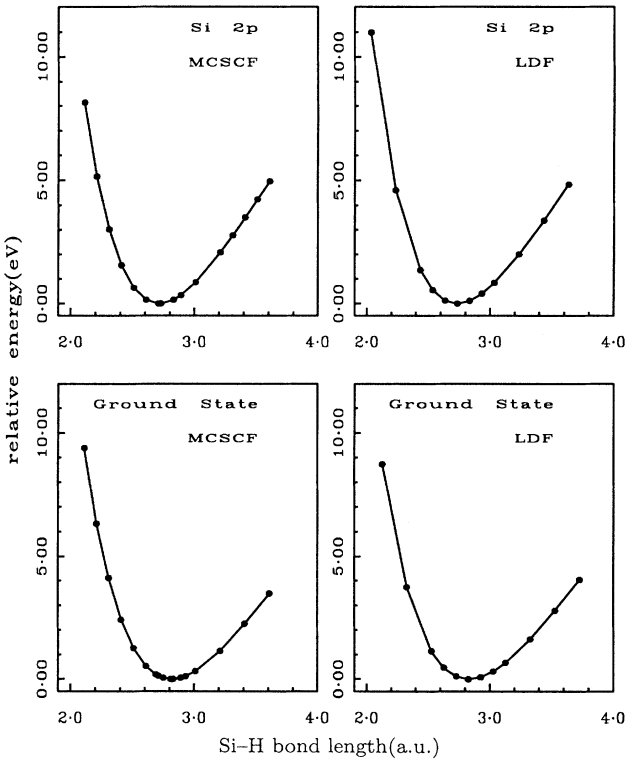

FIG. 1. The calculated potential-energy surfaces for the SiH_4 ground state and the Si $2p$ hole state. The energy labeled is relative to the minimum of each curve. The MCSCF minimums are $-287.354\,615\,7$ a.u. for the Si $2p$ state, and $-291.287\,813\,2$ a.u. for the ground state. The LDF minimums are $-286.697\,118\,3$ a.u. for the $2p$ state, and $-290.688\,839\,1$ a.u. for the ground state.

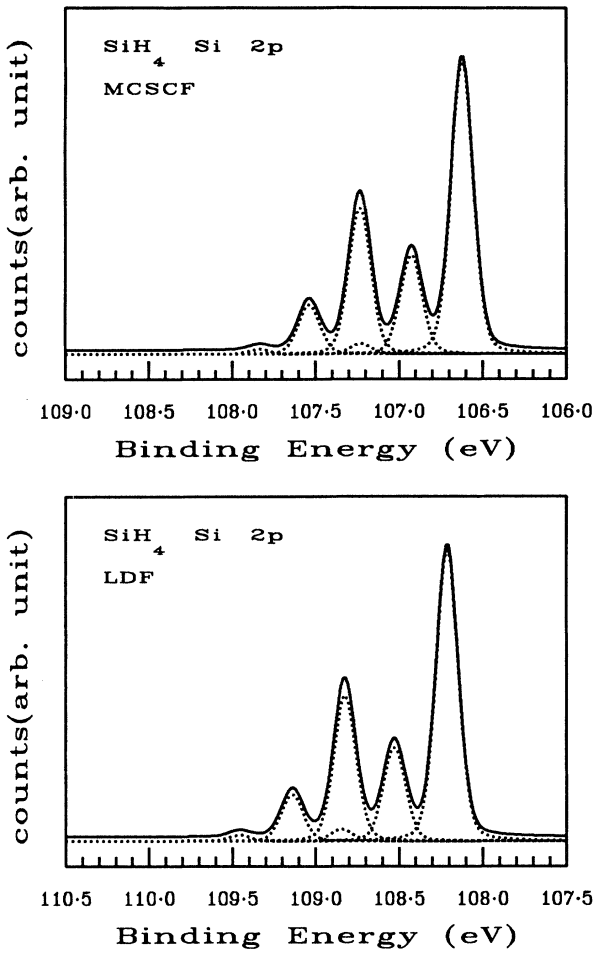

FIG. 2. The calculated Franck-Condon profile for the SiH_4 Si $2p$ hole state. The experimental splitting of 0.61 eV and an intensity ratio of 2:1 are used for the $2p$ hole spin-orbit coupling. The calculated Franck-Condon factors are convoluted for each spin-orbit component with Voigt functions, using a width of 0.15 eV and an 80% Gaussian factor, both obtained from fitting the experimental photoelectron spectrum of SiH_4.

MCSCF calculation has reproduced the dramatic trend from SiH_4 to GeH_4. There is again a reasonable agreement between theory and experiment [6] for GeH_4.

Also listed in Table I and II, and shown in Figs. 1–3, are the results from the LDF calculation. When compared with the experiment, the LDF method is as successful as the MCSCF method in reproducing the Franck-Condon profiles for both SiH_4 and GeH_4, although the MCSCF ionization potentials are in better agreement with the experiment than the LDF results. Good agreement is also found between the MCSCF and LDF results, and the bond distances calculated by the LDF method are only slightly different from those calculated by the MCSCF method. Based on these comparisons, the LDF method has the promise to provide reasonably accurate results for the calculation of core hole states.

B. Calculations for other core levels of SiH_4 and GeH_4

One possible explanation for the observed difference between the SiH_4 Si $2p$ and the GeH_4 Ge $3d$ spectra is that the SiH_4 spectrum is due to a p level (Si $2p$), while the GeH_4 spectrum is due to a d level (Ge $3d$). In other words, it is due to the difference in the angular momentum quantum number of the ionized core orbitals. To explore this possibility, we systematically studied all the core hole states of SiH_4 and GeH_4, using both the MCSCF and LDF methods. The optimized M—H bond lengths for these core hole states are listed in Table I. Both the MCSCF and LDF methods predict that for core levels with the same principle quantum numbers, the contraction of the M—H bond after the core-level ionization is almost the same. For example, the Si—H bond lengths for the Si $2s$ hole state and the Si $2p$ hole state are the same based on the MCSCF results (2.82 a.u.), while the LDF calculations predict an insignificant difference of only 0.007 a.u. in bond length between these two states. The difference between the calculated Franck-Condon profiles of the Si $2p$ and $2s$ hole states is small, as listed in Table II. Thus, based on our calculations, the observed difference between the SiH_4 spectrum (Si $2p$) and the

GeH_4 spectrum (Ge 3*d*) is not due to the angular momentum quantum number of the ionized core levels. Comparison between the calculation results for the GeH_4 Ge 3*d* and 3*p* levels (Table II) also supports this conclusion. The Ge 3*p* level is much deeper than the Ge 3*d* level (Table I), which shows that the very small vibrational structure on the Ge 3*d* level is not due to the low Ge 3*d* binding energy either.

Our calculations also reveal another interesting trend: the Franck-Condon factors for higher vibrational states increase for the core levels with a smaller principle quantum number, i.e., for deep core levels. For example, the vibrational structure increases significantly going from the Si 2*p* and 2*s* levels to the Si 1*s* levels. Experimentally the Si 1*s* vibrational structure will probably never be resolved because of the large inherent linewidth (≥ 0.5 eV) [19] and the even larger photon widths at the present time. The same trend is also predicted for the Ge core levels, but the increase in vibrational structure is not nearly as dramatic as for the Si core levels. Comparing the MCSCF and the LDF calculations, the MCSCF method predicts the same bond length for all core levels with the same principle quantum number, while the LDF method predicts small variations (<0.008 a.u.) within such a group, depending on the angular momentum quantum number. This is also reflected in Table II, which collects all the calculated constants for the vibrational splittings. In essence, both the MCSCF and LDF calculations predict identical bond lengths for all core-level subshells with the same principle quantum number but a substantial contraction of the bond length for the ionization of deeper core levels.

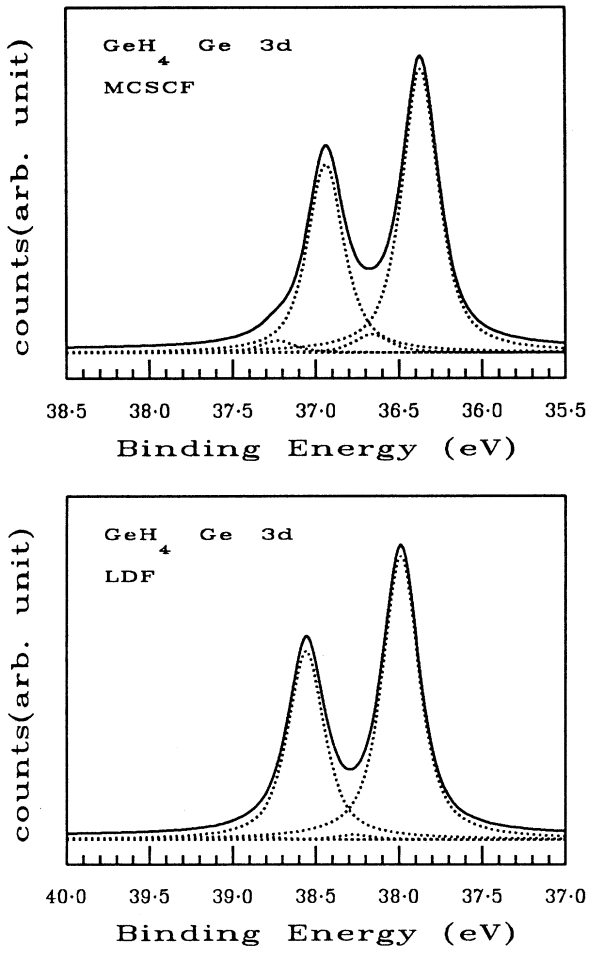

FIG. 3. The calculated Franck-Condon profile for the GeH_4 Ge 3*d* (t_2) hole state. The experimental splitting of 0.57 eV and an intensity ratio of 3:2 are used for the 3*d* hole spin-orbit coupling. The calculated Franck-Condon factors are convoluted for each spin-orbit component with Voigt functions, using a width of 0.25 eV and a 30% Gaussian factor, both obtained from fitting the experimental photoelectron spectrum of GeH_4.

C. Ligand-field splitting of Ge 3*d* in GeH_4

In the tetrahedral environment of GeH_4, the Ge 3*d* levels are split into two components, t_2 and e. Using HBr as an example [20], the ligand-field splitting of the Br 3*d* level is ~ 0.2 eV, largely due to the contribution from the C_2^0 term ($C_2^0 \sim 30$ meV). The contribution from C_4^0 is very small ($C_4^0 \sim 1$ meV). In T_d symmetry, only the small C_4^0 term will contribute to the ligand-field splitting [21,22]. Thus we would expect the ligand-field splitting to be very small for Ge 3*d* in GeH_4. This is supported by the experimental GeH_4 spectrum [6]. The two spin-orbit components are of the same width, indicating that the ligand-field splitting is almost negligible [21].

The LDF calculations predict a splitting of ~ 50 meV between the t_2 and e 3*d* orbitals, as listed in Table I. Considering the width observed in the experimental Ge 3*d* is 0.25 eV, such a splitting would contribute very little to the total linewidth.

However, the ligand-field splitting estimated by the MCSCF calculation is 0.18 eV, which is definitely too large when compared with experiment. Moreover, the equilibrium bond distance of the Ge 3*d* core hole states in t_2 symmetry is 0.02 a.u. longer than that in e symmetry, resulting in a small difference between the Franck-Condon profiles of these two symmetries, as listed in Table II. The MCSCF calculated potential-energy curves for the Ge 3*d* hole states in e and t_2 symmetries are shown in Fig. 4. Such discrepancies are probably due to the incompleteness of the basis set used in the MCSCF calculations. In addition, differential relaxation may have also contributed to these discrepancies due to the inequivalent complete active space for t_2 and e.

D. Jahn-Teller distortions and bending mode vibrations

The Si 2*p* spectrum of SiH_4 and the Ge 3*d* spectrum of GeH_4 differ from the C 1*s* spectrum of CH_4 in that the *p* and *d* orbitals are not in a_1 symmetry. Thus, in addition to symmetric stretching vibrations, the bending mode vibrations could also be excited. The removal of an electron from the degenerate *p* (t_2 in T_d) or *d* orbitals (t_2 and e in T_d) could result in Jahn-Teller distortions, which have been observed in the valence photoelectron spectra of both SiH_4 and GeH_4 [23], because of the vibronic coupling between the degenerate states via the nontotally

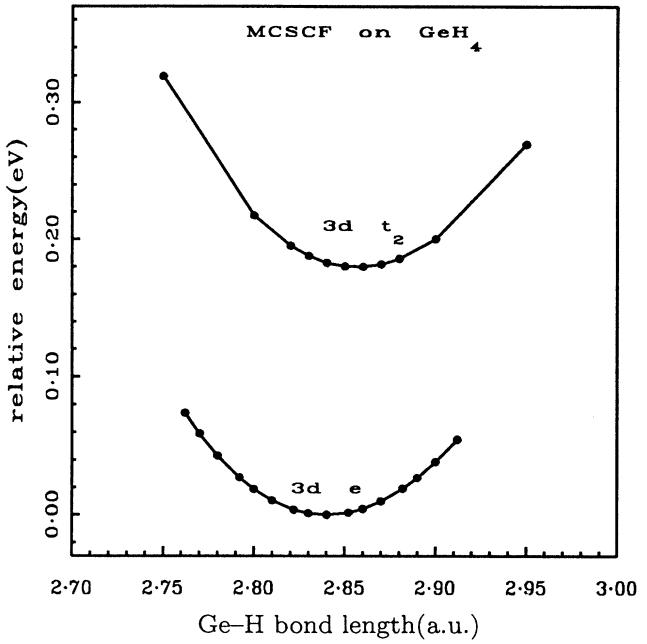

FIG. 4. The MCSCF calculated potential-energy curve for the GeH_4 Ge $3d$ hole state in the T_d t_2 and e symmetries. The minimum of the e curve is at an absolute energy of $-2075.723\,002\,7$ a.u.

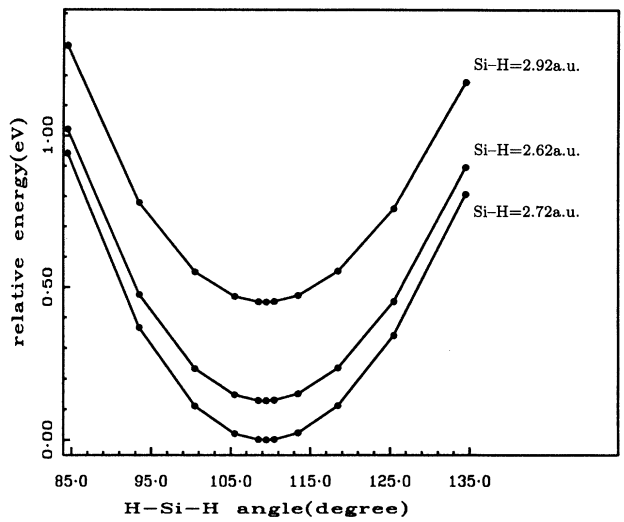

FIG. 5. The MCSCF calculated potential-energy curve for the SiH_4 Si $2p$ hole state in D_{2d} symmetry. The absolute energy at the minimum of the Si—H=2.72 a.u. curve is $-287.354\,615\,7$ a.u., the same as the minimum energy of the $2p$ curve optimized in T_d symmetry, shown in Fig. 1.

symmetric vibrations.

The Jahn-Teller effects can be divided into the static effects, which are due to the change in the potential-energy surface after the ionization, and the dynamic effects, which are due to the vibronic coupling [23]. Although every ionization process affected by the Jahn-Teller distortion is essentially a dynamic process, a calculation of the static Jahn-Teller effects can tell us how important these effects are for a particular ionization process. The Jahn-Teller distortion after the ionization of the t_2 degenerate orbitals can lower the T_d symmetry to C_{3v}, D_{2d}, C_{2v}, or C_s. Using the MCSCF method, we attempted to evaluate the static Jahn-Teller effects by optimizing the geometry of SiH_4^+ with a $2p$ hole in both C_{3v} and D_{2d} symmetries. Since the SIRIUS program can only handle D_{2h} and its subgroups, the C_{3v} calculations have to be performed in C_s symmetry. The calculation results predict a C_{3v} symmetry (instead of T_d) for the ground state of SiH_4, probably due to the incompleteness of the active space. For D_{2d} symmetry, a C_{2v} symmetry is used in the MCSCF calculation and all the Si—H bond lengths are fixed to the same value. The distorted potential-energy surface is evaluated by varying the Si—H bond length, and at each fixed Si—H bond length the H—Si—H angle is changed until a minimum is located. As shown in Fig. 5, for the Si $2p$ core hole state, the geometrical configuration with the lowest energy is Si—H=2.72 a.u., and H—Si—H=109.5°, i.e., the same geometrical configuration obtained in the optimization in T_d symmetry (see Table I). Thus both the excitation to higher bending mode vibrational states and the Jahn-Teller distortions should be small for the Si $2p$ hole state, in agreement with the experimental observation [2,4].

Using the analytical gradient in the DMOL program, we optimized the geometry of both the SiH_4 Si $2p$ hole state and the valence $2t_2$ hole state, in C_{2v} symmetry. For the valence $2t_2$ hole state, the optimized geometry is in D_{2d} symmetry, with a H—Si—H angle of 136.7°, significantly different from T_d symmetry. The most stable symmetry of the SiH_4 $2t_2$ hole state remains controversial in the literature [23,24], and is beyond the scope of this paper. However, the LDF method indeed correctly predicts that the static Jahn-Teller effects are very important for this state. In contrast, the optimized geometry of the Si $2p$ state is again very close to T_d symmetry, with a H—Si—H angle of 109.43°, compared to the value of 109.5° expected for T_d symmetry. These results are consistent with the MCSCF calculations and the experiment.

Our calculations on the Ge $3d$ and $3p$ hole states of GeH_4 also found the most stable geometry is distorted very slightly from the T_d symmetry, indicating a very small static Jahn-Teller effect. However, the dynamic Jahn-Teller effects are much more complicated for the Ge $3d$ level. The two near-degenerate states t_2 and e of different spatial symmetry can interact with each other vibronically via a nontotally symmetrical vibrational mode [25,26]. This may have caused the larger than expected Ge $3d$ width (~ 0.25 eV) observed in the experiment [6].

IV. DISCUSSION

The theoretical results reported above and the experimental results reported in Ref. [6] reveal three periodic trends for the vibrational profiles of the core-level photoelectron spectra of XH_n: the vibrational structure decreases down a group of congeneric molecules, decreases

across a periodic row of isoelectronic molecules, and increases for deep levels with smaller principle quantum numbers. In the present work we have studied vibrational spectra following core ionization with respect to these trends, and have also presented results for different azimuthal quantum numbers for a given principal quantum number. Previous studies of core vibrational spectra have been restricted to one of these trends, namely "across the row" [27]. The first-row C, N, O, and F, containing diatomics, have constituted the prime test cases in addition to a few of the first-row polyatomic molecules [27]. The trends across the first row indicate that C, N, O, and F ionization leads, respectively, to bond shortening, small bond shortening, small bond lengthening, and dissociation. The underlying causes are found in both initial-state (Koopmans, electrostatic) and final-state (relaxation) effects. For C, the initial-state effect dominates; for F the final-state effect dominates; while the effects are roughly of equal importance for N and O ionization.

The trends given above are best rationalized by the vibronic coupling constant, i.e., the final-state energy gradient evaluated at the ground-state equilibrium geometry, since this quantity determines both the bond-length changes and the vibronic excitations. The trends in the three quantities—vibronic coupling constants, bond length changes, and the vibronic excitations—thus correlate through the assumption of harmonic potential surfaces and the linear coupling model for vibronic excitations. As for the ionization potentials themselves, one can subdivide the contributions to the vibronic coupling constants in terms of electrostatic, relaxation, and correlation effects; for heavy-Z elements relativistic effects may also become significant. The first two of these are the most relevant ones; for the first-row period, the electrostatic contribution to the vibronic coupling ("Koopmans's gradients") can be both positive and negative. They are always positive for C and N, can be negative for O, but are always negative for F. The relaxation contribution is always negative, irrespective of the element, and lengthens the bond. Rationalizations of these findings were given previously [28,29]. The electrostatic part derives from a connection between the photoelectron chemical shift and the bonding contributions of core electrons [29]. Taking CO as an example, the charging of the C atom and the decharging of the O atom, respectively, upon stretching of the bond leads to increase (for C) and decrease (for O) of the core ionization potentials (IP's), thus to positive (for C) and negative (for O) core electron vibronic coupling constants, respectively. The sign of the charging is determined by the electropositive or electronegative character. Thus the bond lengthening of oxygen and fluorine compounds derives partly from the electronegative character of these compounds, and partly from the relaxation effect. That the relaxation contribution to the gradient is negative can be rationalized by perturbation theory corrections to Koopman's energy, which involve strongly antibonding orbitals that are unoccupied in the one-particle approximation [28]. For the relaxation part, one must also account for the particular bonding in the resonance valence structures for the core hole ion.

A. Trends across a periodic row

From Table III we note that the results for the presently investigated molecules fall well within the "trends across a periodic row" briefly recapitulated above. Thus C ionization gives a strong positive electrostatic gradient (shortening) of the bond, while relaxation is negative. (Compare "Koopmans" and "SCF" entries in Table III; the gradient values decrease going from "Koopmans" to "SCF", but the absolute SCF values are still positive.) It is interesting to note that both "MCSCF" and "DMOL" entries strengthen the effect of relaxation; that is a further lengthening of the bond. Again this might be rationalized in that beyond the one-particle approximation (here correlation) one must consider the population of low-lying antibonding orbitals; and the correlation, like relaxation, gives a lengthening of the bond.

The isoelectronic hydrides (XH_n) across a periodic row, such as SiH_4, PH_3, H_2S, and HCl or CH_4, NH_3, H_2O, and HF, follow the above stated trends: less shortening going from C (or Si), N (or P), O (or S), and F (or Cl). (Actually for O and F, the bond length is increased after $1s$ ionization [27].) One can anticipate that the particular type of bonding will play a role. The participation of the valence X s orbital in the X—H bonding decreases from SiH_4 to HCl. In the case of SiH_4, the Si valence orbitals form four equivalent Si—H bonds by sp^3 hybridization, while in HCl, and Cl contribution to the Cl—H bond is almost entirely due to the Cl $3p_z$ orbital. When a core hole is created, the s orbital contracts more than the p orbitals, and would thus contribute more to the relaxation effect. Such effects can also be important in the preedge photoabsorption spectra, especially for transitions to the nonbonding Rydberg orbitals [30].

In the "across the row" rationalization, one can also consider the $Z+1$ or the resonance-valence-structure approximation, in which the core-ionized species is replaced by its equivalent core species. The findings for the first-row species are fairly well rationalized by this approximation, e.g., that nitrogen bonds are shorter than carbon bonds, or that the equivalent $F(1s^{-1})$ core, Ne, is inert and leads to dissociation. The entries in Table III indicate that, for the presently investigated molecules, the $Z+1$ approximation gives the correct magnitudes and trends. The trends are in all cases overestimated, just as is the case for first-row species [27].

TABLE III. The derivatives of ionization potentials versus the X—H bond distances for CH_4, SiH_4, and GeH_4 at the experimental equilibrium bond distances (in atomic units).

	Koopmans	SCF	$Z+1$	MCSCF	DMOL
CH_4 $1s$[a]	0.268	0.174	0.213	0.1477	0.1498
SiH_4 $2p$	0.146	0.0993	0.1616	0.0866	0.0785
SiH_4 $2s$	0.145	0.1002	0.1616	0.0877	0.0739
SiH_4 $1s$	0.193	0.1373	0.1616	0.1246	0.149
GeH_4 $3d$	0.091	0.0648	0.1108	0.0395	0.0121
GeH_4 $2p$	0.109	0.0810	0.1108	0.0592	0.0666
GeH_4 $1s$	0.1231	0.0921	0.1108	0.0745	0.0606

[a]The CH_4 calculation was performed using the same basis set as in Ref. [10] and the same active space as SiH_4.

B. Trends down the shells for one element

There are distinct differences in the vibronic coupling constants for different principal quantum numbers, as seen for SiH_4 and GeH_4 in Table III. The radial wave function of a core orbital is largely determined by the principal quantum number. The smaller the principal quantum number, the more tightly bound to the nucleus is the core orbital, and the more it contributes to the shielding. Thus, using SiH_4 as an example, the removal of a Si $1s$ core electron decreases the shielding more than the removal of a $2s$ or $2p$ electron. Related to the shielding is the penetration of valence charges through the core, i.e., there is a differential charge penetration for the $n=1$, 2, and 3 shells. These different penetrations induce slightly different chemical shifts in the x-ray photoelectron spectra, and are also manifested directly in the chemical shifts observed in core-core x-ray emission spectra [31]. We associate this initial-state electrostatic penetration effect as before the main source for the difference in vibronic coupling constants between the main shells. Both absolute and differential charge penetrations change with geometry, thereby contributing to the energy gradient. However, as seen in Table III, the relaxation contributions are also significantly different for different main shells.

C. Trends down the column

For a group of congeneric molecules, the total number of electrons increases down a column of the Periodic Table. For example, the number of core electrons is 10 in SiH_4, and 28 in GeH_4. In the ionization process, one electron is removed from a core level. The larger the number of total core electrons, the smaller is the decrease of the shielding (formed by all the core electrons) after the core-level ionization, and the smaller the alteration of the M—H (M=Si,Ge) bond. Related to the screening are the core-valence Coulomb integrals which in turn relate to the correlation constant in the electron spectroscopy for chemical analysis (ESCA) potential model for core electron chemical shifts [32]. The smaller the size of this integral the higher the Z; this might be one rationalization for the Koopmans gradient decreasing with increasing Z. Also with an increase of Z the relaxation contribution diminishes. It is, however, interesting to note from Table III that the ratio between electrostatic and relaxation contributions is fairly constant down the column.

According to Slater's rules, the screening constant is larger for the inner shells than for the valence shells. But for subshells derived from the same principal quantum number, their screening constants are the same. It is also well known that the effective screening of atoms in the same period increases with atomic number due to poorer screening of the valence electrons. Consequently, also from the notion of screening constants, the M—H bond lengths can be expected to alter more for deeper core levels and also for lighter elements within the same period. In this connection, it is interesting to note that the $Z+1$ approximation overestimates the M—H bond alteration in all cases, but least so for the deepest core level.

Although these trends have only been elucidated here for hydride molecules, they should be generally valid for many other ligands. For example, we already know that Si molecules such as SiF_4 give a larger vibrational profile than for Ge or Sn analogs [3], or for Xe or I molecules [33,34]. These trends then should hold widely for many adsorbates, solids, and gases, although it must be realized that so far, in addition to the first-row diatomics [27] we have only considered high-symmetry molecules where the symmetric stretch dominates the vibrational structures.

V. CONCLUSION

Theoretical (MCSCF and LDF) results are in agreement with the trends observed experimentally: core-level vibrational structure decreases dramatically, both down a group of congeneric molecules, and across a periodic row of isoelectronic molecules.

The calculated Franck-Condon profiles for the Si $2p$ spectrum of SiH_4 and the Ge $3d$ spectrum of GeH_4, by both the MCSCF and LDF methods, are in semiquantitative agreement with the experiment. The LDF method thus provides an alternative to the more time-consuming MCSCF method for the study of the dynamics of core-level ionization, especially for large molecules.

Theoretical calculations also show that the vibrational structure increases for deep core levels with a small principal quantum number, and that bending mode vibrations and the static Jahn-Teller effects are small for the Si $2p$ spectrum of SiH_4 and the Ge $3d$ spectrum of GeH_4.

These trends, which are generally valid for absorbates, solids, and gases, can be rationalized by the factors determining the shielding effect of the core electrons.

We have analyzed the observed trends by computing the vibronic coupling constants at different levels of approximations, and analyzed the contributions of electrostatic, relaxation, and correlation effects to these constants. It is found that in all cases the relaxation, and correlation contributions to the vibronic coupling constant are negative, i.e., bond lengthening. The electrostatic contributions in all cases make strong positive contributions, outweighing the two former contributions and giving the net effect of a considerably shortened bond. We find also the electrostatic contribution to be the major fact that governs all the "across the row," "down the column," and "down the shell" trends.

ACKNOWLEDGMENT

We thank the Natural Sciences and Engineering Research Council (NSERC) of Canada for financial support.

[1] G. M. Bancroft, J. D. Bozek, J. N. Cutler, Y. F. Hu, Z. F. Liu, D. G. Sutherland, K. H. Tan, and J. S. Tse, in *Proceedings from the Tenth International Conference on Vacuum Ultraviolet Radiation Physics,* edited by F. J. Weilleumier, Y. Petroff and I. Nenner (World Scientific, Singapore, 1993), pp. 191–200.
[2] J. D. Bozek, G. M. Bancroft, J. N. Cutler, and K. H. Tan, Phys. Rev. Lett. **65**, 2757 (1990).
[3] J. D. Bozek, G. M. Bancroft, and K. H. Tan, Phys. Rev. A **43**, 3597 (1991).
[4] D. G. J. Sutherland, G. B. Bancroft, and K. H. Tan, Surf. Sci. **262**, L96 (1992).
[5] D. G. J. Sutherland, Ph.D. thesis, the University of Western Ontario, 1993.
[6] Z. F. Liu, J. N. Cutler, G. M. Bancroft, K. H. Tan, R. G. Cavell, and J. S. Tse, Phys. Rev. A **46**, 1688 (1992); S. Svensson, A. Ausmees, S. J. Osborne, G. Bray, F. Gel'mikhanov, H. Agren, A. Naves de Brito, O. P. Sairanen, A. Kivimäki, E. Nommiste, H. Aksela, and S. Aksela, Phys. Rev. Lett. **72**, 3021 (1994).
[7] B. O. Roos, Adv. Chem. Phys. **69**, 399 (1987).
[8] H. J. A. Jensen, H. Ågren, and J. Olsen, in *Modern Techniques in Computational Chemistry: MOTECC-90,* edited by E. Clementi (ESCOM, Leiden, 1990).
[9] R. G. Parr and W. Yang, *Density-Functional Theory of Atoms and Molecules* (Oxford University Press, New York, 1989).
[10] L. Asplund, U. Gelius, S. Hedman, K. Helenelund, K. Siegbahn, and P. E. M. Siegbahn, J. Phys. B **18**, 1569 (1985).
[11] T. H. Dunning, Jr. and P. J. Hay, in *Modern Theoretical Chemistry,* edited by H. F. Schaefer III (Plenum, New York, 1977), Chap. 1.
[12] T. H. Dunning, Jr., J. Chem. Phys. **66**, 1382 (1977).
[13] S. Huzinaga, J. Chem. Phys. **42**, 1293 (1965).
[14] L. D. Landau and E. M. Lifshitz, *Quantum Mechanics,* 3rd ed. (Pergamon, New York, 1976).
[15] J. W. Rabalais, *Principles of Ultraviolet Photoelectron Spectroscopy* (Wiley, New York, 1977).
[16] *DMol User Guide,* Biosym, April, 1990.
[17] L. Versluis and T. Ziegler, J. Chem. Phys. **88**, 3322 (1988).
[18] *Structure Data of Free Polyatomic Molecules,* edited by K. H. Hellwege and A. M. Hellwege (Springer-Verlag, Berlin, 1987).
[19] M. O. Krause, J. Phys. Chem. Ref. Data **8**, 307 (1979).
[20] Z. F. Liu, G. M. Bancroft, K. H. Tan, and M. Schachter, J. Elect. Spectrosc. Relat. Phenom. **67**, 299 (1994).
[21] J. N. Cutler, G. M. Bancroft, J. D. Bozek, and K. H. Tan, J. Chem. Phys. **97**, 7932 (1992).
[22] B. N. Figgis, *Introduction to Ligand Fields* (Interscience, New York, 1966), pp. 38–40.
[23] J. H. D. Eland, *Photoelectron Spectroscopy: An Introduction to Ultraviolet Photoelectron Spectroscopy in the Gas Phase,* 2nd ed. (Butterworths, London, 1984).
[24] T. Kudo and S. Nagase, Chem. Phys. **122**, 233 (1988).
[25] L. S. Cederbaum, J. Chem. Phys. **78**, 5714 (1983).
[26] R. L. Fulton and M. Gouterman, J. Chem. Phys. **35**, 1059 (1961).
[27] J. Müller and H. Ågren, in *Proceedings of the NATO ASI Conference on Molecular Ions,* edited by J. Berkowitz (Plenum, New York, 1980).
[28] O. Goscinski and A. Palma 322 (1977).
[29] H. Ågren, Chem. Phys. Lett. **75**, 1267 (1981).
[30] Z. F. Liu, G. M. Bancroft, J. S. Tse, and Z. Z. Yang, Chem. Phys. (to be published).
[31] R. Manne, in *Inner-Shell and X-Ray Physics of Atoms and Solids,* edited by D. J. Fabian *et al.* (Plenum, New York, 1981).
[32] K. Siegbahn, C. Nordling, G. Johansson, J. Hedman, P. F. Heden, K. Hamrin, U. Gelius, T. Bergmark, L. O. Werme, R. Manne, and Y. Baer, *ESCA Applied to Free Molecules* (North-Holland, Amsterdam, 1969).
[33] J. N. Cutler, G. M. Bancroft, and K. H. Tan, J. Phys. B **24**, 4897 (1991).
[34] J. N. Cutler, G. M. Bancroft, K. H. Tan, and G. J. Schrobilgen, J. Am. Chem. Soc. **113**, 9125 (1991).